Exploiting Isotope Effects to Improve Fluorophores

Jonathan B. Grimm, Natalie Falco, Heejun Choi, Frank Xie, T.C. Binns, James Liu, Jennifer Lippincott-Schwartz, and Luke D. Lavis*
Janelia Research Campus, Howard Hughes Medical Institute, 19700 Helix Drive, Ashburn, Virginia, U.S.A.

Introduction

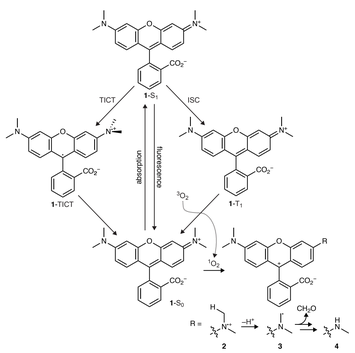

Figure 1: Photophysics of tetramethylrhodamine (**TMR**, **1**)

Rhodamine dyes such as tetramethylrhodamine (**TMR**, **1**, **Figure 1**) remain in wide use due to their excellent brightness, superb photostability, and broad spectral range.[1-3] The photophysics of rhodamines are well understood due to their importance as biological probes and laser dyes.[4] Absorption of a photon excites the TMR molecule from ground state (**1**-S_0) ultimately to the first excited state (**1**-S_1). After excitation, the molecule can relax back to the S_0 through a variety of processes. Emission of a photon (fluorescence) competes with nonradiative decay pathways such as twisted internal charge transfer (TICT) where electron transfer from the aniline nitrogen to the xanthene system gives a charge-separated species (**1**-TICT) that rapidly decays back to the ground state (**1**-S_0) without emitting a photon.[5] This process competes with fluorescence, thereby decreasing fluorescence quantum yield (Φ). Alternatively, the excited dye can undergo intersystem crossing to the first triplet excited state (**1**-T_1) where it can sensitize singlet oxygen ($^1O_2$), returning to the ground state (**1**-S_0). The resulting $^1O_2$ can then react with the ground state of the dye, oxidizing the aniline nitrogen to a radical cation (**2**), which can undergo deprotonation to a carbon-centered radical (**3**) that ultimately results in dealkylation of the dye to form trimethylrhodamine (**4**).[4] This process results in a blue-shift in absorption (λ_{max}) and emission (λ_{em}) maxima, which can complicate multicolor experiments and is a prelude to additional dealkylation and irreversible photobleaching steps.

Rhodamines

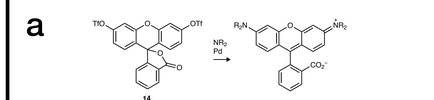

dye	**1**	**5**	**6**	**7**	**8**	**9**	**10**	**11**	**12**	**13**
X	H	D	H	D	H	D	H	D	H	D
λ_{max} (nm)	548	547	549	548	553	554	560	559	545	544
λ_{em} (nm)	572	570	571	570	576	576	586	586	574	575
ε ($M^{-1}cm^{-1}$)	78,000	94,500	101,000	96,700	76,000	104,000	80,000	92,600	84,000	87,800
Φ	0.43	0.50	0.88	0.86	0.70	0.80	0.08	0.12	0.11	0.13

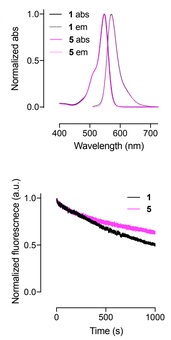

Figure 2: Spectral properties and photobleaching of rhodamine derivatives

We envisioned another strategy to increase brightness and photostability of small-molecule fluorophores such as **1** by replacing the hydrogen (H) atoms on the *N*-alkyl groups with deuterium (D). Deuterated alkylamines exhibit higher ionization potentials relative to their hydrogen-containing analogs,[6] suggesting that deuteration could decrease the efficiency of the TICT process and therefore increase quantum yield. This higher ionization potential could also slow the initial electron abstraction step (*i.e.*, **1** ▶ **2**) and the stronger C–D bond could slow the rate of deprotonation (*i.e.*, **2** ▶ **3**, **Figure 1**), together decreasing the efficiency of the dealkylation step. We tested this hypothesis that deuteration of *N*-alkyl groups would improve brightness and photostability by synthesizing a series of rhodamine dyes and their deuterated counterparts (**5**–**13**) using a cross-coupling approach starting from fluorescein bistriflate (**14**; **Figure 2a**).[7] We compared TMR (**1**) and its deuterated analog **5**, finding remarkably similar absorption maximum (λ_{max}) and fluorescence emission maximum (λ_{em}; **Figure 2a**) for the two dyes with no change in the shape of the absorption peak (**Figure 2b**). Deuteration improved the brightness and photostability, however, with **5** showing a ~20% increase in both the extinction coefficient at λ_{max} (ε) and Φ compared to **1** (**Figure 2a**) and slower rate of photobleaching (**Figure 2c**). Based on this result, we investigated other matched pairs of rhodamine dyes with H- or D-containing cyclic *N*-alkyl groups (**6**–**13**). We observed increases in ε and Φ for all the deuterated analogs except for the azetidine-containing rhodamine (**13**), which suggests that azetidination and deuteration affect the same nonradiative decay pathways (presumably TICT; **Figure 1**).

Performance

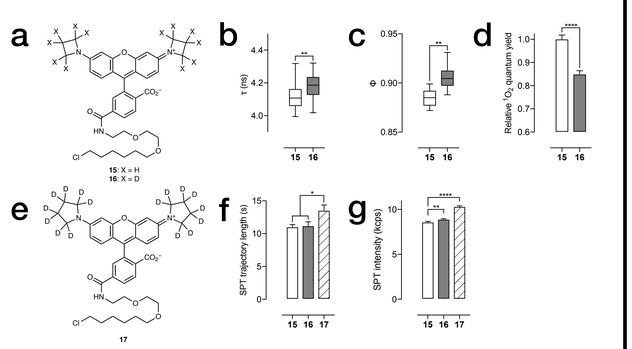

Figure 3: Structures and performance of HaloTag ligands **15**–**17** *in vitro* and in cells.

We then tested these dyes as protein conjugates *in vitro* and in living cells, first synthesizing the HaloTag[8] ligands of the bright azetidinyl-rhodamines (**15** and **16**; **Figure 3a**). We compared their fluorescence properties when attached to HaloTag protein, finding that that the conjugates of the deuterated dye **16** showed longer fluorescence lifetime in cells (τ; **Figure 3b**) and higher fluorescence quantum yield *in vitro* (**Figure 3c**) compared to the nondeuterated **15**. This result suggests that deuteration suppresses a protein-bound-specific mode of nonradiative decay. Surprisingly, deuteration also significantly suppressed $^1O_2$ generation (**Figure 3d**). Based on the high brightness of the deuterated pyrrolidine-containing rhodamine **9** (**Figure 2a**) we also synthesized the HaloTag ligand of this compound (**17**; **Figure 3e**). We compared HaloTag ligands **15**–**17** in live-cell single-particle tracking experiments using sparsely expressed Sox2–HaloTag fusions.[9] Deuteration of the azetidine showed no improvement in photostability in cells (*i.e.*, average track length of individual molecules; **Figure 3f**), but the deuterated pyrrolidine rhodamine ligand **17** did show significantly longer tracks compared to azetidinyl dyes **15** and **16**. Deuteration did elicit a higher brightness (*i.e.*, photons/s, **Figure 3g**) with conjugates of both **16** and **17** emitting more photons per unit time compared to the conjugate of **15** under equivalent imaging conditions.

C- and Si-Rhodamines

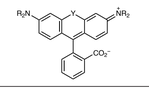

Y	$C(CH_3)_2$				$Si(CH_3)_2$			
dye	**18**	**19**	**20**	**21**	**22**	**23**	**24**	**25**
X	H	D	H	D	H	D	H	D
λ_{max} (nm)	608	608	613	612	646	645	652	650
λ_{em} (nm)	631	628	633	633	664	662	668	667
ε ($M^{-1}cm^{-1}$)	99,000	111,000	87,000	130,000	5,600[a]	8,600[a]	12,600[a]	17,600[a]
Φ	0.67	0.74	0.54	0.70	0.54	0.54	0.48	0.53

[a]ε value in 10 mM HEPES, pH 7.3; ε > 150,000 $M^{-1}cm^{-1}$ in EtOH with 1% v/v TFA

Figure 4: Spectral properties of carborhodamines **18**–**21** and Si-rhodamines **22**–**25**.

We then applied this modification to other rhodamine analogs, focusing on the azetidine and pyrrolidine modifications based on the high brightness observed for the rhodamines **7** and **9** (**Figure 2**). For both the azetidinyl- and pyrrolidinyl-carborhodamines[10] **18** and **20**, we observed substantial increases in both Φ and ε when the cyclic amines were deuterated to give **19** and **21** (**Figure 4**). We then examined the Si-rhodamines **22** and **24** and their deuterated analogs **23** and **25**. As with the rhodamine series, deuteration of the azetidinyl rhodamine **22** to give **23** did not elicit a large increase in fluorescence quantum yield (Φ), although the extinction coefficient in water (ε) was modestly increased. Deuteration of the pyrrolidine-containing rhodamine **24** to give **25** did elicit a substantial increase in both Φ and ε, in line with the rhodamine series (**Figure 2**).

Performance

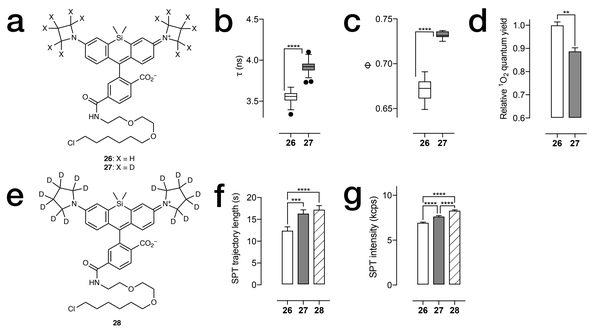

Figure 5: Structures and performance of HaloTag ligands **26**–**28** *in vitro* and in cells.

We then synthesized the HaloTag ligands of the azetidinyl Si-rhodamine compounds (**26** and **27**, **Figure 5a**) and measured the effect of deuteration *in vitro* and in living cells. Like the analogous rhodamine compounds (**Figure 3**), the deuterated azetidinyl dye **27** showed showed increased fluorescence lifetime (τ) as the HaloTag conjugate inside live cells (**Figure 5b**) and a substantial increase in Φ compared to **26** when attached to the HaloTag (**Figure 5c**); compound **27** also gave lower $^1O_2$ generation (**Figure 5d**). We also prepared the deuterated pyrrolidinyl Si-rhodamine HaloTag ligand (**28**, **Figure 5e**). In live-cell single-molecule experiments using cells sparsely expressing Sox2–HaloTag fusion proteins,[9] we discovered that the HaloTag conjugates of deuterated dyes **27** and **28** were both more photostable than the conjugates of nondeuterated **26**, with deuterated pyrrolidine Si-rhodamine **28** showing the longest average single-molecule track length (**Figure 5f**). Likewise, the conjugates of the deuterated dyes exhibited higher brightness with **28** showing the highest photons/s (**Figure 5g**).

Other Dyes

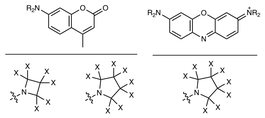

dye	**29**	**30**	**31**	**32**	**33**	**34**
X	H	D	H	D	H	D
λ_{max} (nm)	354	353	381	381	655	653
λ_{em} (nm)	467	469	472	472	671	669
ε ($M^{-1}cm^{-1}$)	15,000	15,500	19,800	19,700	85,000	85,000
Φ	0.96	0.89	0.46	0.56	0.16	0.22

Figure 6: Spectral properties of coumarins **29**–**32** and oxazines **33**–**34**.

Finally, we applied the deuterium substitution to other dyes beyond tetramethylrhodamine analogs. We first explored the coumarin scaffold, synthesizing the azetidinyl coumarins **29** and **30** and the pyrrolidinyl pair **31** and **32** (**Figure 6**). Consistent with the other dyes, the spectral properties of the deuterated azetidine compound **30** was similar to the parent **29** with similar ε and a small decrease in Φ. For the pyrrolidinyl compounds the differences were more pronounced, with deuterated dye **32** showing significantly higher Φ compared to **31**; the ε for the two dyes was equivalent. We also synthesized the pyrrolidinyl oxazine compound **33** and deuterated congener **34**. Like the other pyrrolidine-containing dyes, the deuterium substitution caused a substantial increase in Φ.

References

(1) Lavis, L. D.; Raines, R. T. *ACS Chem. Biol.* **2008**, *3*, 142–155. (2) Beija, M.; Afonso, C. A. M.; Martinho, J. M. G. *Chem. Soc. Rev.* **2009**, *38*, 2410–2433. (3) Lavis, L. D.; Raines, R. T. *ACS Chem. Biol.* **2014**, *9*, 855–866. (4) Zheng, Q.; Lavis, L. D. *Curr. Opin. Chem. Biol.* **2016**. (5) Grimm, J. B.; English, B. P.; Chen, J.; Slaughter, J. P.; Zhang, Z.; Revyakin, A.; Patel, R.; Macklin, J. J.; Normanno, D.; Singer, R. H.; Lionnet, T.; Lavis, L. D. *Nat. Methods* **2015**, *12*, 244–250. (6) Hull, L. A.; Davis, G. T.; Rosenblatt, D. H.; Williams, H. K. R.; Weglein, R. C. *J. Am. Chem. Soc.* **1967**, *89*, 1163–1170. (7) Grimm, J. B.; Lavis, L. D. *Org. Lett.* Synthesis of rhodamines from fluoresceins using Pd-catalyzed C-N cross-coupling. **2011**, *13*, 6354–6357. (8) Los, G. V.; Encell, L. P.; McDougall, M. G.; Hartzell, D. D.; Karassina, N.; Zimprich, C.; Wood, M. G.; Learish, R.; Ohana, R. F.; Urh, M. *ACS Chem. Biol.* HaloTag: A novel protein labeling technology for cell imaging and protein analysis. **2008**, *3*, 373–382. (9) Liu, Z.; Legant, W. R.; Chen, B. C.; Li, L.; Grimm, J. B.; Lavis, L. D.; Betzig, E.; Tjian, R. *eLife* 3D imaging of Sox2 enhancer clusters in embryonic stem cells. **2014**, *3*, e04236. (10) Grimm, J. B.; Sung, A. J.; Legant, W. R.; Hulamm, P.; Matlosz, S. M.; Betzig, E.; Lavis, L. D. *ACS Chem. Biol.* Carbofluoresceins and carborhodamines as scaffolds for high-contrast fluorogenic probes. **2013**, *8*, 1303–1310.